Impact of Late Quaternary climatic fluctuations on coastal systems: Evidence from high-resolution geophysical, sedimentological and geochronological data from the Java Island

Franto Novico, David Menier, Manoj Mathew, Mu Ramkumar, M. Santosh, Cipta Endyana, Kresna Tri Dewi, Indra Kurniawan, Clément Lambert, Evelyne Goubert

Version of Record: https://www.sciencedirect.com/science/article/pii/S026481722100502X
Manuscript_1678c0ab96dd876c3c209c8c460ab039

Impact of Late Quaternary climatic fluctuations on coastal systems: Evidence from high-resolution geophysical, sedimentological and geochronological data from the Java Island

Franto Novico[1,2], David Menier[3,*], Manoj Mathew[4], Mu Ramkumar[5], M. Santosh[6,7], Cipta Endyana[1], Kresna Tri Dewi[8], Indra Kurniawan[9], Clément Lambert[3], Evelyne Goubert[3], Hendarmawan[1]

[1]Department of Engineering Geology, Padjadjaran University, 45363 Jatinangor, Indonesia

[2]Marine Geological Research and Development Center, Ministry of Energy and Mineral Resources, 40174 Bandung, Indonesia

[3]Laboratoire Géoscience Océan, UMR CNRS 6538, Université Bretagne Sud, 56017 Vannes, France

[4]Laboratoire Géoscience Océan, UMR CNRS/UBO/UBS 6538, IUEM, Université de Brest, 29280 Plouzané, France

[5]Department of Geology, Periyar University, 636011 Salem, India

[6]Department of Earth Sciences, University of Adelaide, Adelaide, SA 5005, Australia

[7]Beijing School of Earth Sciences and Resources, China University of Geosciences, 100083 Beijing, China

[8]Center of Geological Survey, Ministry of Energy and Mineral Resources, 40122 Bandung, Indonesia

[9]Directorate of Water Resources, Ministry of Public Works and Housing, 12110 Jakarta, Indonesia

*Corresponding author: david.menier@univ-ubs.fr (D. Menier).

Abstract

The major climatic oscillations during the Quaternary Period significantly influenced the evolution and distribution of ancient and modern coastal systems. Here we investigate the morphology and sedimentary infilling of submerged Late Quaternary incised valleys along the northern coast of Java Island (Indonesia) using high-resolution geophysical, sedimentological and geochronological data. Our results indicate that the spatial development and morphology of the incised valleys are predominantly controlled by Quaternary glacial–interglacial eustatic fluctuations, within a marked subsiding setting. The valleys were incised during prominent Quaternary lowstands and most of the valley fill was emplaced during the last postglacial sea level rise. The valley fill forms a transgressive succession, consisting mainly of fluvial deposits at the base (possibly amalgamated from older sequences) overlain by shallow marine sediments and capped by hemipelagic deposits. The valley-fill architecture is strongly dependent on the valley morphology (depth of incision, width of the valleys, and extent of the intertidal zone). The shallow marine deposits contained within the narrow and linear valleys are mostly aggrading muds. The vertical incision and valley formation was chiefly controlled by the extent of glacial sea-level fluctuations. The studied sections represent the continental-offshore extension of a paleodeltaic system. The implication of our work is that even in predominantly enclosed shallow marine systems that are located distal to the shelf break, the response of the sedimentary system and ensuing stratigraphic configuration can be effectively impacted by the rapid and abrupt Quaternary global climatic transition and eustatic sea-level fluctuations.

Keywords: Last Glacial Maximum; Java Sea; Incised Valleys; depositional controls; stratal morphology

1. Introduction

The Quaternary Period is characterized by rapid, large-scale and abrupt climatic oscillations that strongly influenced the evolution and distribution of ancient coastal systems around the world and continue to exert control until present-day (Adams et al., 1999; Elias, 2013; Gornitz, 2021). The associated eustatic fluctuations predominantly generated arrays of incised valleys during relative sea level lowstands which were inundated and filled during subsequent relative sea level rise, inundated and infilled the incised valleys. Over the last 40 years, owing to its scientific and economic significance, extensive research has been focused on the stratigraphy and infilling of such incised valleys or paleochannels (Puchala et al., 2011; Wang et al., 2020). Research conducted elsewhere has provided important geomorphologic as well as stratigraphic information from regions such as the North and South American shelf (e.g., Dalrymple et al., 1994; Nordfjord et al., 2006; Moreira et al., 2019), northwest European shelf (e.g., Allen and Posamentier, 1993 and 1994; Tesson et al., 2000; Chaumillon et al., 2010; Menier et al., 2010; Martinez-Carreno and Garcia-Gil, 2017), northeastern Australian shelf (e.g., Fielding et al., 2005), southwestern Huanghai shelf (e.g., Kong et al., 2011), South African shelf (e.g., Green, 2009), eastern Indian coast (e.g., Dubey et al., 2019), Sunda shelf in Southeast Asia (e.g., Hanebuth et al., 2009; Puchala et al., 2011; Horozal et al., 2021), among others.

In Southeast Asia, the Sunda Shelf or Sundaland is an extension of the continental shelf and includes the island of Java, the Malay peninsula, Sumatra, Borneo, Madura, Bali and their surrounding smaller islands. It covers an area of approximately 1.85 million km². Its seas are relatively shallow and was exposed several times during the Pleistocene (e.g., Emery et al., 1972; Hanebuth et al., 2009) when Sumatra, Java, Borneo and the Malay peninsula were connected and formed a single large landmass (Heaney et al., 1991; Voris, 2000; Bird et al., 2005) (Fig. 1A). During the Last Glacial Maximum (LGM), ~26.5–19 ka BP, much of the remaining Sundaland area was covered by savanna, grassland, lowland evergreen forests, marshy grounds and crossed axially by the deeply incised ‘rivers’ feeding the late falling-stage deltas that debouched close to the present-day shelf break of the Sundaland (Hanebuth et al., 2009; Hanebuth et al., 2011; Puchala et al., 2011; Sathiamurthy and Rahman, 2017; Irwanto, 2019). The Java Sea that today corresponds to a large and shallow sea of the Sunda Shelf, which lies between the islands of Borneo to the north, Java to the south, Sumatra to the west and Sulawesi to the east, was entirely exposed during the LGM (Clark et al., 2009). The Java Sea was occupied by river valleys and channels that coursed to the shelf break located toward the eastern part of Java. Currently, the northwestern region of the Java Sea hosts a poorly-documented offshore sedimentary prism dominated by argillaceous deposits within a rapidly subsiding geodynamic setting (Abidin et al., 2008, 2013 and 2015, Chaussard et al., 2013; Husson et al., 2019). While it is recognized that this region has undergone various phases of tectonic and eustatic fluctuations until recent-times (e.g., Zahirovic et al., 2016), a detailed analysis of the sedimentary architecture and stratigraphic archive, which can potentially encapsulate evidences of important environmental changes in response to endogenic and exogenic forcing, remain less understood.

Here, we present a detailed description of the shallow sub-bottom stratigraphy of the offshore section of northwest Java (Fig. 1B) using results obtained from shallow seismic surveys and cores collected in 2015. These results, aided with radiocarbon ages provide insights into the Pleistocene to Holocene transition events and the major climatic and eustatic controls on the sedimentary organization within a subsiding shelf setting.

2. Geological characteristics of Java and Java Sea

2.1. Structural setting

Sundaland consists of a stable core of Paleozoic continental crust that was augmented in size by tectonism and volcanism associated with subduction along the southern margin of the continent, with episodes of uplift and subsidence affecting the entire Sunda Shelf (Bird et al., 2005; Metcalfe, 2011). Java represents a volcanic arc built on the southernmost margin of the continental Sunda Plate, due to the subduction of the oceanic Australia-Indian plate (Fig. 2A; Hamilton, 1979). It is a structurally complex island attributable to a long history of accretion of Gondwana-derived crustal blocks that led to a configuration of alternating highs and transverse depressions (Haberland et al. 2014). The northern part of the Northwest Java Basin, including the coastal area, is dominated by extensional faulting with minimal compressional structures (Darman and Sidi, 2000; Sathiamurthy et al., 2006). It was formed by continuous subsidence and southward tilting of the Sunda Plate since the Paleogene (Hamilton, 1979). The subsidence is documented to have resulted in the development of the Pulau Seribu carbonate platforms (Fig. 1B) and the NE-SW trending asymmetrical northwest Java basinal area (Suyanto et al., 1977). Subsequent development of several sub-basins and basement highs within the basin (Patmosukismo et al., 1974) was associated with N-S trending block faulting (Adriansyah et al., 2002).

2.2. Geomorphology and seafloor sedimentary cover

Morphologically, the Java Sea is roughly rectangular in shape, located between Sumatra to the west and Bali to the east. In the west, it is open to the Indian Ocean through the Sunda Strait and the Karimata Strait, respectively. In the east, it has an open connection to the Flores Sea and the Sulawesi Sea through the Makassar Strait (Durand & Petit, 1995; Genia et al., 2007). The Java Sea including Jakarta Bay is a large (~310,000 km^2), shallow sea (40–100 m water depth) and the slope is toward the east at the edge of the Sunda Shelf. Seafloor surface sediment of Indonesian waters including the Java Sea generally consists of cohesive fine-grained sediments (Fig. 2).

Java presents an elongated morphology with a surface area of ~130,000 km^2 (~1000 km in length and ~210 km wide). The coastline is structurally controlled and shows an irregular morphology. Northern Java including the Jakarta Bay is in a transition area between the volcanic arc and the extensional back-arc zone. This area is characterized by the flat alluvial plain of the coastal zone. The southern parts of Java are occupied by volcanic mountains where Mount Semeru is the highest (~36576 m). Java is drained by multiple rivers, with large drainage basins in the north and small drainage basins in the south (Figure 3). The drainage pattern is predominantly controlled by the volcanic arc and recent uplift (Marliyani, 2016).

2.3. Sea level changes

On a global scale, the development of Quaternary stratigraphy of continental shelves was predominantly controlled by glacio-eustatic fluctuations (Suter et al., 2012). Hence, an understanding of relative sea-level change may help to explain critical interactions in earth environmental systems throughout the Quartenary (Shennan, 2018).

The Sundaland core is considered to be tectonically quiescent, as evidenced by the lack of noticeable seismic activity of the fault systems. However, a recent biographical study on organism divergence time (Husson et al., 2019) shows that Sundaland was subaerially exposed before 400 ka and subsequently experienced subsidence at a rate of 0.2–0.3 mm yr^{-1} (Sarr et al., 2019). The insights gained from Sarr et al. (2019), resulted in an updated framework of sea level changes for Sundaland by combining variations of both glacio-eustatic and subsiding activity.

During the LGM, when ice sheets were at their maximum, the glacio-eustatic depression of the sea level by ~120 m had fully exposed the Sunda Shelf. Several previous studies (e.g., Bird et al., 2005; Sathiamurthy et al., 2006; Cannon et al., 2009; Sathiamurthy et al., 2017), using sedimentological, geophysical and palynological data records from the LGM stage, reconstructed the paleogeography of Sundaland along the areas from the South China Sea and Malacca Strait to the Java Sea. The area was dominated by large fluvial drainage systems with savanna and lowland evergreen vegetation in their catchment areas (Fig.1A). Sea level changes seem to play a critical role in variability of the sedimentary successions in these areas including the Jakarta Bay and the Java Sea.

The last marine flood that initiated ~19 ka BP had significant consequences on the remobilization of sediments of the paleolandscapes associated with the vast coastal plain, which occupied most of the present-day Java Sea. During this sea level rise, the new hydrodynamic conditions led to a reorganization of the sedimentary architecture that initiated with continental sedimentary regime to a mixed sedimentary system (i.e., both marine and continental) and then culminated in an exclusively marine-dominated stratigraphic architecture, to reach the current coastline of northern Java.

3. Material and methods

3.1. Geophysical data acquisition and processing

Two high-resolution reflection seismic (HRRS) single channel data records were used. The first set of seismic profiles correspond to refined HRRS campaigns that were carried out in June to July 2015, covering nearly the entire Jakarta Bay. The second set of seismic profiles were obtained from the HRRS data acquisition campaign that was conducted in March 1990 (unpublished report by Kurnio et al., 1991) for the Java Sea (Fig. 1B). Both seismic records were acquired by deploying a sparker system that could penetrate up to 250 ms TWTT. Cheaspeake Sonarwiz 5 software was used for processing the single channel data by completing the sea bottom track by noise attenuation, seismic signal gaining by Automatic Gain Control and User Define Gain/Attenuation, bandpass filtering through frequency selection to have a better resolution of seismic reflectors at upper layers of sub-sea bottom and seismic trace stacking by increasing the ratio of signal/noise to obtain a better quality of the reflectors. The time-depth conversion for sediment unit boundaries was assumed using an internal velocity of 1600 m/s beneath the seafloor (Puchala et al., 2011; Martínez-Carreño and García-Gil, 2017). Thus, 200 m depth was reached with some approximately visible reflectors. Survey positioning was achieved with a differential global positioning system (DGPS) using CNAV 3050. The seismic reflectors were analyzed following the procedures enlisted by Mitchum and Vail (1977), Brown and Fisher (1980), Posamentier et al. (1988), Posamentier and Vail (1988), and Catuneanu (2019).

3.2. Sediment cores

Ten boreholes (BH-01–BH-10) were drilled (Figs. 1C and 2B) around the Jakarta Bay. The borehole, BH-10, has the deepest water depth (22 m below Lowest Astronomical Tide -LAT), while the others varied from 14 to 19 m water depth below LAT. Among the 10 boreholes, the drilling depth of BH-02 and BH-07 reached 150 m below the sea bed and both boreholes were located in the middle of the bay (Fig. 1C and Table 1). The other boreholes were drilled to a depth of 60 m below the seafloor. The retrieved sediment cores were used to describe the lithology, microfauna and organic matter (e.g., fragments of fossilized wood, rootlets, charcoal, etc.) to decipher the depositional environments, which were interpreted based on granulometric analyses (30 g dry samples were sieved for grain sizes 2 mm, 500 µm, 250 µm and 63 µm) and microfossil analysis (using stereo zoom Zeiss Stemi SV 11) following standard procedures.

3.3. AMS ^{14}C dating

The selected samples for radiocarbon dating were analyzed with Accelerator Mass Spectrometry at the Radiocarbon Laboratory, University of Arizona, USA. Each age measurement was conducted on shell fragments and organic matter extracted from the cores. All radiocarbon dates are given in years before present/1950 (BP) (Smith et al., 2011; Reimer et al., 2013). Radiocarbon dates with a “measured radiocarbon age” older than 46,400 yrs BP are outside the detection limits and are not calibrated; thus, these ages are shown as > 46,400 yrs BP (Table. 2).

4. Results

4.1. Interpretation of seismic reflection configuration patterns and seismic stratigraphy

The seismic profiles were analyzed in terms of continuity, amplitude, configuration and termination of reflectors following Mitchum et al. (1977) and Catuneanu (2019). This was followed by the recognition of seismic units and description of the recognized units along with their boundaries (unit boundary - UB). The characteristics of the acoustic facies are summarized in Table 3 for the seismic units observed in the offshore zone and identified in boreholes BH-02 and BH-07.

To illustrate the Holocene infilling of the incised valleys from the Jakarta Bay to the Java Sea, we selected five seismic profiles that are located in the central part of the study zone.

In the five profiles (sparker profiles: L-42, CL-06B, L-C7, L-C8 and L-X), located at water depths ranging from 5 to 50 m, seven seismic units, i.e., U1–U7, from the base towards the top, were identified in the sedimentary infilling of the incised valleys (Fig. 4 and Table 3). These units are illustrated on the selected profiles, except for Units 1, 2 and 3, which are only adequately visible on L-42. Units 1 and 2 are characterized by discontinuous reflectors with an acoustically opaque configuration.

Unit 1 (U1) is located in the basal part (Fig. 4A) and displays a thickness of >25 ms TWTT (>20 m). The reflectors of U1 demonstrates very poor continuity, low frequency and low amplitude (Table 3). The reflection configuration is aggrading sub-parallel with attenuated zones (acoustically opaque) as a result of subsurface gas. It should be noted that this area has been shown to contain acoustically turbid zones, which are related to the presence of gas in organic-rich sediments (e.g., Schubel, 1974; Baltzer et al., 2005).

Unit 2 (U2) presents an acoustic thickness varying from 20 to 35 ms TWTT (~16 m to 28 m). Continuity, amplitude and frequency in seismic facies range from low to medium and very poor at some parts with acoustic turbidity (Table 3). Reflector configuration displays aggrading sub-parallel to parallel patterns associated with a shallow marine environment, such as a deltaic depositional system.

Unit 3 (U3) exhibits an acoustic thickness varying between 35 ms to 60 ms TWTT (~28 m to 48 m). U3 is characterized by aggrading reflectors in the sedimentary prism wedging morphology systems towards the south and the north, particularly in the lower section of the seismic line L42. This seismic facies is interpreted as a deltaic depositional system.

Unit 4 (U4) overlies U3 (Figs. 4 and 5) and has an acoustic thickness varying between 50 ms and 70 ms TWTT (~40 m to 64 m). The reflectors show very poor to moderate continuity and the amplitude and frequency are medium (Table 3). The top of the unit is bounded by an erosional surface. The internal reflectors show corrugated reflector stacking pattern, probably due to the prevalence of superimposed subaqueous lobes within a deltaic system, and some erosional surfaces, which in turn are located at the southern and northern parts. The seismic facies could suggest that U4 comprises an alluvial plain depositional environment (Reineck and Singh, 1980; Catuneanu et al., 2009; Catuneanu, 2019).

Unit 5 (U5) overlies U4 with an acoustic thickness varying between 5 ms to 50 ms (~4 m to 40 m) and is bounded by erosional surfaces on the top and bottom (Figs. 4 and 5). The unit extends laterally to a planar geometry. The continuity of seismic facies is very poor to poor corresponding to acoustic attenuation and demonstrates an oblique-aggrading subparallel geometry, while amplitude and frequency are low to high (Table 3). Aggrading subparallel seismic reflector geometry is commonly found beside discontinuous reflectors that could indicate existing gas pockets. This unit presents a general organization of horizontal reflectors with some downlap and onlap in a few places. Using indications from the seismic facies, the depositional environment of U5 is interpreted as a delta plain with some parts containing alluvial channels and tidal flat sediments (Brown and Fisher, 1980; Reineck and Singh, 1980; Catuneanu et al., 2009; Catuneanu, 2019).

The next unit, U6, presents an acoustic thickness of 5 ms to 40 ms TWTT (~4 m to 32 m) (Figs. 4 and 5). This unit reveals acoustic facies that are characterized by aggrading parallel and progradation pattern of poor continuity, and low to high frequency with very low to high amplitude (Table 3). The base of U6 corresponds to a subaerial unconformity and demonstrates flat upper layers that overlie clinoform deposits in some parts (Figs. 4 and 5), which intersects U5 with a divergent filling pattern. The variation in thickness of this unit is associated with incised channels and U6 is interpreted as delta front deposits within a shallow marine setting (Reineck and Singh, 1980; Dalrymple et al., 2003; Catuneanu et al., 2009; Catuneanu, 2019).

Unit 7 (U7) is the most recent seismic unit which overlies U6 (Figs. 4 and 5). The seismic facies show medium to good continuity with good amplitude and medium frequency. Seismic reflector configuration is predominantly aggrading parallel (Table 3). The acoustic thickness ranges between 5 ms to 30 ms TWTT (~4 m to 24 m). The depositional environment of U7 is interpreted as a subaqueous fan delta in the south-central and eastern parts that can be associated with existing river mouths and a shoreface setting toward the north as seen in the modern bathymetric map of the study area.

4.2. Lithofacies description and correlation from sediment cores

Lithofacies description of the recognized seismic units was conducted on selected cores, i.e., BH-02, BH-04, BH-05, BH-06, BH-07 and BH-09 (Figs. 2B and 6). It is evident from the sparker profile L-42 (Fig. 4A) that these cores represent a complete and continuous record of stratigraphic successions in units U2 to U7, and thus provide the optimal opportunity to investigate the sedimentary infilling history of the study area. U2 was recognized at a depth of 130–150 m and consists of dark grey to olive grey silt and clay, and medium to dark grey very-fine to fine-grained sand and the depositional environment indicated an inner shelf setting. U3 comprises of sediments that correspond to grey clay and dark grey medium-grained sand as seen in BH-02 and BH-07 and gathering information from the seismic facies, this unit is interpreted as being deposited in a deltaic setting. The lithology of U4, as seen in cores BH-04 to BH-09, and identified at a depth of 46–100 m below the seabed, is characterized by dark grey to olive grey silt with traces of clay, medium to coarse grain greyish brown sand and silt with traces of clay that indicate a shallow marine to alluvial plain depositional environment. Core description of boreholes BH-04 and BH-09 (Fig. 6) reveal that U5 consists predominantly of greyish brown to brown sand and brownish grey silt and clay. Informed by the seismic facies and lithofacies, we interpret the depositional environment of U5 as a delta plain with some parts containing alluvial channels and tidal flat sediments. The sediments of U6, witnessed in the boreholes BH-05 and BH-07, reveal dark grey to black sand, medium to coarse grained sand and dark grey mud with some medium grain sand. The basal sequence boundary is overlain by yellowish-brown medium grain sand, reversed graded bedding, containing shell fragments, which denote a shallow marine to deltaic depositional environment. U7 occupies the stratigraphic succession between 0 to 12 m and consists of yellowish-grey clay with medium grained sand containing visually ±10% of shell fragments and depositional environment is interpreted as a shallow offshore environment

4.3. Micropaleontological indices

Microfossils were identified and described from cores BH-02, and BH-07 (Table 4).

The dominant benthic foraminifera taxa (i.e., *Ammonia* spp .; *Asterorotalia* spp.) (Fig. 7 and Table 4) in U2 seem to indicate a coastal waters environment. *Ammonia tepida* is indeed known to be tolerant to continental organic matter and freshwater inputs in the southwestern Pacific region (Debenay, 2012). *Asterorotalia* spp. is a typical warm water epifaunal benthic foraminifera well represented in riverine influx dominated coastal domain (Panchang and Nigam, 2012; Saraswat et al., 2017). Microfossil barren zones are observed in U4 in both BH-02 and BH-07. A gradual increase in benthic foraminifera, especially *Elphidium* spp., *Operculina* spp. and *Quinqueloculina* spp. is seen in the upper parts of U4 and in U5 within BH-07, while ostracods are very rare in these two units (Table 4). Similarly, in BH-02, the lack of ostracods is evident in U4 and U5, while rare occurrences of *Elphidium* spp., *Pseudorotalia* spp. and *Quinqueloculina* spp. is noticed in upper parts of U4. U6, similar to U3, entails an abundance of various species of ostracods and benthic foraminifera and this could be indicative of a shallow marine setting (Table 4). U7 reveals the presence of some marine benthic foraminifera taxa found in modern warm marine waters of southwestern Pacific Ocean (e.g. *Dendritina* spp., *Spiroloculina* spp., Hohenegger et al., 1999; Debenay, 2012). *Dendritina* spp. is indeed a full marine species frequently found abundant in regions protected from extreme hydrodynamic forcing.

4.4. Radiocarbon ages

A total of 3 cores (i.e., BH-05, BH-06 and BH-07) were sampled for radiocarbon dating. The dating analysis from a sample recovered at 134.5 m depth of BH-07 and pertaining to U2 revealed an age of > 49,900 ka BP.

In the same core, ^{14}C dating results (Table 2) of samples at 77 m depth and 56.2 m depth, and within U4, presented ages of > 46.4 ka BP and 41.8 ± 1.5 cal ka BP, respectively.

The result of radiocarbon dating applied on shell materials of the sub-sample from 14.3 m below the seabed from BH-06 revealed an age of 8461 ± 29 cal yrs BP (Table 2).

The dating applied on molluscan shell collected at 7 m depth below seafloor from BH-05 returned an age of 3,308 ± 24 cal yrs BP (Table 2).

5. Discussion

5.1. Sequence stratigraphic framework

While all the depositional units are not equally preserved in all the studied valleys, a general stratigraphic scheme can be drawn that applies over the entire zone or system.
The chronology of the complete succession remains speculative for Units 1, 2 and 3 except for the upper units (U4–7), wherein, the formations indicate ages ranging from the Pleistocene to Holocene. U4 that signifies the falling stage systems tract shows a first stage of incision and is characterized by alluvial deposits (Figs. 4 and 6), which indicate ages of > 46.4 ka BP and 41.8 ± 1.5 cal ka BP (MIS 3) (Table 2) and we interpret this sequence to be associated with the accumulation of regressional deposits following the persistent drop of relative sea level since MIS 5e. The microfossil assemblages (benthic foraminifera and ostracods) within U4 show a dramatic decline in BH-02 and BH-07 (Table 4) that further supports the interpretation of relative sea level drop and subaerial exposure of the shelf. U5 incorporates mixed fluvio-estuarine deposits that could have been emplaced initially under lowered relative sea levels, during which, regressional alluvial channel deposits continued to accumulate and sealed the first incisional features. Incision synchronously propagated across these deposits, and later as relative sea level began to gradually increase there could have been reduced incisional capacity with aggradation of sediments due to a rise in base level and some filling

of the incised system, and owing to these evidences, we deduce U5 to represent the lowstand systems tract. The gradual rise in sea level and estuarine sedimentation is corroborated by the increase in population of brackish and saline water favoring benthic foraminifera species such as *Elphidium* spp., *Operculina* spp. and *Quinqueloculina* spp. in BH-07. U6, demonstrating an age of 8461 ± 29 cal yrs BP (Table 2) in the intermediate part of the sequence and which lies above the transgressive surface, consists of shallow marine sediments that may have been deposited during rapid transgression after ~15 ka BP, which could efficiently preserve the preceding fluvial deposits, and we posit that this unit elucidates the transgressive systems tract. Lastly, the Holocene sediments forming the hemipelagic drape of U7 that overlie the maximum flooding surface represent the highstand systems tract.

5.2. Valley morphology

As defined by the seismic data shown in figure 5 (Fig. 1B for location), the valleys run parallel to the coast and are between 1 and 10 km long. They follow a regional slope towards the shelf break and reach maximum depths of ~30 to 40 m. These valleys are increasingly wide towards the east, particularly where several valleys converge, and are linked to the confluence of fluvial channels. Indeed, there could have been high rates of sedimentation, channel flow and drainage discharge which could possibly explain the processes of alluviation and incisional dynamics that promoted the notable widening of the emerging valleys in the Java Sea (Fig. 8), that are mainly controlled by global sea level changes during the LGM (Voris et al, 2000; Hanebuth et al., 2004; Clark et al, 2009; Sar et al, 2019).

These valleys, filled by marine transgressive deposits (U6–shallow marine), are underlain by mixed fluvio-estuarine formations of weakly consolidated origin (U5–lowstand channel fill), the facies of which are mainly fine to medium grained.

The morphology of the valleys demonstrates generally a flat bottom and markedly steep edges (Fig. 5).

The morphology with a flat bottom and marked edge can be explained by the lithological nature of the incised unit (U5), consisting of weakly consolidated and easily remobilized alluvial plain deposits, and conversely as a zone where the potential for incision is very low given the low to medium slopes in a region very far from the continental slope (Fig. 8A). The incision depths of ~8 m to 32 m, (Fig. 5) are of the same order as those documented from other parts of the world, for example, on the platforms of the American east coast (Thomas and Anderson, 1994; Foyle and Oertel, 1997), the Bay of Biscay (Lericolais et al., 2001; Chaumillon et al., 2008; Chaumillon et al. 2010; Menier et al., 2010; Estournès et al., 2012; Menier et al., 2014; Martínez-Carreño and García-Gil, 2017), the Mediterranean (Tesson et al., 2010; Tesson et al., 2015), India (Dubey et al., 2019) and also in Southeast Asia (Hanebuth, et al., 2009; Puchala et al., 2011; Alqahtani, et al., 2015; Wang et al., 2020; Horozal et al., 2021).

5.3. Depositional evolution

The main stratigraphic units recognized across the study area are composed of continental formations (U4 and U5) that transitions upward to shallow marine deposits (U6 and U7). This interpretation is also confirmed by the succession of fossil foraminifera faunas, from taxa that are indicative of environments under continental influence (*e.g. Asterorotalia* spp.) to those that are indicators of shallow coastal waters (*e.g. Dendritina* spp., *Spiroloculina* spp., *Operculina* spp.) (Fig. 7 and Table 4). The core and the major parts of the valley fills are composed of alluvial deposits (U5) and shallow marine deposits (U6 and U7), and the vertical facies succession is predominantly deposited within a transgressive setting.

In our proposed model of valley morphogenesis, the supposed thalweg, which overlays the erosional surface UB-4, is dated at 41800 +/- 1500 cal. age BP, which corresponds to the last and deepest incision (pre-LGM incision), and therefore, the overlaying fluvial deposits (U5) could be younger than 25 ka. Based on deductions implied in previous studies (e.g., Posamentier and Allen, 1999; Posamentier, 2001), the alluvial channels more than likely formed when the shelf was not fully subaerially exposed and the lowstand fluvial system was incapable of substantially efficient downcutting, both laterally and vertically.

On the seismic records (Fig. 3B and Table 3) U4 seem to illustrate an irregular and oblique aggrading subparallel or wavy reflector geometry and we interpret it as interfluves or bars, dominated by sandy to silt-argillaceous facies established during the marine isotopic stage 3 (Fig. 9).

Unit 5 is interpreted to consist of lowstand channel fill deposits that accumulated during periods of significant drops in sea level but the majority during the post lowstand system tract (LST), which was lower than present-day in this zone (Fig. 9). Our results clearly highlight the occurrence of alluvial channel deposits and nearshore tidal flat sediments that are explicitly indicative of a shift from a relatively sand-rich lowstand system to a clay-rich nearshore sediment as mention in Table 4. Gathering consensus from the global and Sunda shelf sea level curves (Fig. 9), the transition from a fluvial to a shallow marine setting in our data could correspond to the post-LGM abrupt and rapid sea level rise induced by deglaciation. Furthermore, our inference of an abrupt and rapid rise in sea level is congruent with previous findings (Hanebuth et al., 2000) of an accelerated increase in eustatic levels in the northern Sunda Shelf during the MWP 1A (meltwater pulse) event that commenced at ~14.7 ka and terminated before ~13.8 ka, including an abrupt rise of up to ~16 m within a span of 300 years that occurred between 14.6–14.3 ka cal BP (Hanebuth et al., 2000).

Unit 6, dated at ~8461 +/- 29 cal. age BP, which mainly rests above Unit 5, is interpreted as deposited in the course of the last sea level rise over the area (Fig. 8). As the fluvial valleys were flooded by the rising sea levels, sediment supply could not keep pace with the increase of accommodation space, and this would explain the aggrading nature of Unit 6. The very homogeneous structure of Unit 6 and the inferred fine-grained sedimentation would point to a wave-dominated bay (Dalrymple et al., 1994). While there is an inexistence of sandy barriers in the seismic record, the Java Sea seems to be a sector that was very calm, favoring low-energy sedimentation comparable to that in estuarine central basins (lagoonal basins). Further expanding on our sedimentological and seismic data, we favor the interpretation of very calm and low-energy conditions in the Java Sea during the deposition of Unit 6. We base this on an additional line of evidence, viz. the preservation of Unit 5 could be plausible only under rapid transgression and placid hydrodynamic environments. This can effectively weaken potential erosional processes, given that ubiquitously, the efficient preservation of lowstand fluvial deposits, subsequent to erosion during transgression and reworking by inclement hydrodynamic conditions, would be, at best, in patches (Allen, 1991; Allen and Posamentier, 1993; Posamentier, 2001).

Unit 7 is interpreted as offshore muds aggrading above the estuarine valley fills as the first succession overlaying UB-6. It rests above the maximum flooding surface that truncates all the units below (Figs. 4 and 10). The unit is dated at ~3308 +/- 24 yr BP, and is composed of Holocene-age hemipelagic drape. U7 was emplaced during a full transgression over the area, inasmuch as it overlaps most of the valley interfluves.

6. Conclusions

Two remarkable incisions are identified in the Java Sea shelf. The first incision occurred during the sea level drop of the marine isotopic stage 3, which was later sealed by lowstand alluvial channel deposits. These deposits were re-incised during the LGM, creating the second incisional surface. This discontinuity does not intersect the Upper Pleistocene incision, indicating a relatively low incision potential, in a context of rapid sea level rise within very sheltered hydrodynamic conditions.

The incised valleys demonstrate a wide and flat bottom morphology along with very steep edges owing to low velocity channel flow and shallow paleo-topographic gradients. The sedimentary infill of the incised valleys indicates the continent-offshore extension of the paleodeltaic system, complete with variable facies characteristics and variable rates of deposition. Influences of regional slope and hydrodynamics are recognized to have exercised control over the spatial distribution of facies types as well as grain sizes of the facies types.

Prevalence of major river systems that drained the Sundaland Craton that advanced over former offshore regions during LGM created an extensive incised valley and associated geomorphic-sedimentary infill.

Author Contributions

Author Contributions: Conceptualisation: F.N., D.M., M.M., H. and C.E.; methodology: F.N., D.M., R.K. and M.S.; field investigation: F.N. and I.K.; manuscript preparation: F.N., D.M., M.M., M.R. and H.; review and editing: F.N., D.M., M.M., M.R., M.S. and C.E.; figures: D.M., M.M., F.N.,. and C.E.; microfossil analysis: F.N. and K.T.D.

Acknowledgements

The field activities were fully supported by the Ministry of Public Works and Housing, the Republic of Indonesia, under the grant bearing the contract number HK.02.03/PPK-PP/SBBWSCC/1311.2 and also by the Ministry of Energy and Mineral Resources, the Republic of Indonesia, under the contract number P.P.G.L. G.F. 030.90. We also acknowledge the Embassy of France in the Republic of Indonesia and M. Jean-Charles BERTHONNET for providing the funding for the AMS analysis through the ‘Programme Science and Impact’ (March 2017) initiative. M.M. was supported by the ISblue project, Interdiciplinary Graduate School for the blue planet (ANR-17-EURE-0015) and by a grant from the French Government under the program “Investissements d’Avenir”. We express our gratitude to Ir. Duddy Ranawijaya for significantly contributing to improve the manuscript.

References

Abidin, H.Z., Andreas, H., Djaja, R., Darmawan, D., Gamal, M., 2008. Land subsidence characteristics of Jakarta between 1997 and 2005, as estimated using GPS surveys. GPS Solutions 12, 23-32.

Abidin, H.Z., Andreas, H., Gumilar, I., Sidiq, T.P., Fukuda, Y., 2013. On the roles of geospatial information for risk assessment of land subsidence in urban areas of Indonesia. In: Zlatanova, S., Peters, R., Dilo, A., Scholten, H. (eds.), Intelligent Systems for Crisis Management. Lecture Notes in Geoinformation and Cartography. Springer, Berlin, Heidelberg, 277-288.

Abidin, H.Z., Andreas, H., Gumilar, I., Brinkman, J.J., 2015. Study on the risk and impacts of land subsidence in Jakarta. Proceedings of the International Association of Hydrological Sciences 372, 115–120.

Adams, J., Maslin, M., Thomas, E., 1999. Sudden climate transitions during the Quaternary. Progress in Physical Geography 23(1), 1-36.

Adriansyah, A., McMechan, G.A., 2002. Case History, Analysis and Interpretation of seismic data from thin reservoirs: Northwest Java Basin, Indonesia. Journal of Geophysics 67 (1), 14-26.

Allen, G.P., 1991. Sedimentary processes and facies in the Gironde estuary: A Recent model for macrotidal estuarine systems. In: Smith, D.G., Reinson, G.E., Zaitlin, B.A. and Rahmani, R.A. (eds.), Clastic tidal sedimentology. Canadian Society of Petroleum Geologists Memoir 16, 29–40.

Allen, G.P., and Posamentier, H.W., 1993, Sequence stratigraphy and facies model of an incised valley fill: the Gironde Estuary, France. Journal of Sedimentary Petrology 63, 378–391.

Allen, G.P. and Posamentier, H.W. 1994. Transgressive facies and sequence architecture in mixed tide- and wave-dominated incised valleys: example from the Gironde estuary. France. In: Dalrymple, R.W., Zaitlin, B.A. and Boyd, R. (eds.), Incised valley systems: origin and sedimentary sequences. Society of Economic Paleontologists and Mineralogists, Special Publications 51, 225-240.

Alqahtani, F.A., Johnson, H.D., Jackson, C.A.-L, Som, M.R.B., 2015. Nature, origin and evolution of a Late Pleistocene incised valley-fill, Sunda Shelf, Southeast Asia. Sedimentology 62, 1198–1232.

Baltzer, A., Tessier, B., Nouze, H., Bates, R., Moore, C., Menier, D., 2005. Seistec seismic profiles: A tool to differentiate gas signatures. Marine Geophysical Researches 26, 235-245.

Bird, M.I., Taylor, D., Hunt, C., 2005. Palaeoenvironments of insular Southeast Asia during the Last Glacial Period: a savana corridor in Sundaland? Quaternary Science Reviews 24, 2228-2242.

Brown, L.F. and Fisher, W.L., 1980. Seismic-stratigraphic interpretation of depositional systems and its role in petroleum exploration. AAPG Continuing Education Course Notes Series 16, 1-181.

Catuneanu, O., Abreu, V., Bhattacharya, J.P., Blum, M.D., Dalrymple, R.W., Eriksson, P.G., Fielding, C.R., Fisher, W.L., Galloway, W.E., Gibling, M.R., Giles, K.A., Holbrook, J.M., Jordan, R., Kendall, C.G.St.C., Macurda, B., Martinsen, O.J., Miall, A.D., Neal, J.E., Nummedal, D., Pomar, L., Posamentier, H.W., Pratt, B.R., Sarg, J.F., Shanley, K.W., Steel, R.J., Strasser, A., Tucker, M.E., Winker, C., 2009. Towards the standardization of sequence stratigraphy. Earth-Science Reviews 92, 1-33.

Catuneanu, O., 2019. Scale in sequence stratigraphy. Marine and Petroleum Geology 106, 128–159.

Chaumillon, E., Proust, J.N., Menier, D., Weber, N., 2008. Incised-valleys morphologies and sedimentary-fills within the inner shelf of the Bay of Biscay (France): A synthesis. Journal of Marine Systems 72, 383-396.

Chaumillon, E., Tessier, B., Reynaud, J.Y., 2010. Stratigraphic records and variability of incised valleys and estuaries along French coasts. Bulletin de la Société Géologique de France 181, 75-85.

Chaussard, E., Amelung, F., Abidin, H., Hong, S-H., 2013.Sinking cities in Indonesia: ALOS PALSAR detects rapid subsidence due to ground water and gas extraction. Remote Sensing of Environment 128, 150-161.

Clark, P.U., Dyke, A.S., Shakun, J.D., Carlson, A.E., Clark, J., Wohlfarth, B., Mitrovica, J.X., Hostetler, S.W., McCabe, A.M., 2009. The Last Glacial Maximum. Science 325, 710-714.

Dalrymple R.W., Boyd, R., Zaitlin, B.A., 1994. History of research, types and internal organization of incised-valley systems: introduction to the volume. In: Dalrymple, R.W., Boyd, R.J., Zaitlin, B.A. (eds.), Incised-valley systems: origin and sedimentary sequences. Society for Sedimentary Geology special publication 51, 5–12.

Dalrymple, R.W., Baker, E.K., Harris, P.T., Hughes, M.G., 2003. Sedimentology and stratigraphy of a tide-dominated foreland-basin delta (Fly River, Papua New Guinea). In: Sidi, F.H., Nummedal, D., Imbert, P., Darman, H., Posamentier, H.W. (eds.), Tropical Deltas of Southeast Asia-sedimentology, Stratigraphy, and Petroleum Geology. SEPM 76, 147-173.

Darman, H. and Sidi, F.H., 2000; An outline of the geology of Indonesia. Indonesian Association of Geologists, IAGI, Jakarta, 192 pp.

Dubey, K.M., Chaubey, A.K., Mahale, V.P., Karisiddaiah, S.M., 2019. Buried channels provide keys to infer Quaternary stratigraphic and paleo-environmental changes: A case study from the west coast of India. Geoscience Frontiers 10, 1577-1595.

Durand, J.R. and Petit, D., 1995. The Java Sea environment. in: BIODYNEX: Biology, Dynamics, Exploitation of the small pelagic fishes in the Java Sea. Potier, M. and Nurhakim, S. (eds.), Java Sea Pelagic Fishery Assessment Project. AARD/ORSTOM, 14-38.

Elias, S.A., 2013. The Quaternary. Reference Module in Earth Systems and Environmental Science, Elsevier. DOI: https://doi.org/10.1016/B978-0-12-409548-9.05350-1.

Emery, K.O., Uchupi, E., Sunderland, J., Uktolseja, H.L, Young, E.M., 1972. Geological structure and some water characteristics of the Java Sea and adjacent continental shelf. CCOP Technical Bulletin 6, 197-221.

Estournès, G., Menier, D., Guillocheau, F., Le Roy, P., Paquet, F. and Goubert, E., 2012. The paleo-Etel River incised valley on the Southern Brittany inner shelf (Atlantic coast, France): Preservation of Holocene transgression within the remnant of a middle Pleistocene incision? Marine Geology 329-331, 75–92.

Fielding, C.R., Trueman, J.D., Alexander, J., 2005. Sharp-based, flood dominated mouth bar sands from the Burdekin River Delta of northeastern Australia: extending the spectrum of mouth-bar facies, geometry, and stacking patterns. Journal of Sedimentary Research 75, 55–66.

Foyle, A.M. and Oertel, G.F., 1997. Transgressive systems tract development and incised-valley fills within a Quaternary estuary shelf system: Virginia inner shelf, USA. Marine Geology 137, 227–249.

Genia, A.N., Nugroho, A.S., Olugbenda, J.O., 2007. Introduction to Java Sea. Oceanography. Stavanger, University of Stavanger.

Gornitz, V., 2021. Timescales of climate change. In: Alderton, D., Elias, S.A. (Eds.), Encyclopedia of Geology (second edition). Academic Press, pp. 318-327.

Green, A.N., 2009. Palaeo-drainage, incised valley fills and transgressive systems tract sedimentation of the northern KwaZulu-Natal continental shelf, South Africa, SW Indian Ocean. Marine Geology 263, 46-63.

Haberland, C., Bohm, M., Asch, G., 2014. Accretionary nature of the crust of Central and East Java (Indonesia) revealed by local earthquake travel-time tomography. Journal of Asian Earth Sciences 96, 287–295.

Hamilton, W., 1979. Tectonics of the Indonesian region. United State of Geological Survey, Washington, 1078 pp.

Hanebuth, T., Stattegger, K., Grootes, P.M., 2000. Rapid flooding of the Sunda Shelf: A Late-Glacial sea-level record. Science 288, 1033-1035.

Hanebuth, T.J.J., Stattegger, K., Bojanowski, A., 2009. Termination of the last glacial maximum sea-level lowstand: the Sunda-Shelf data revisited. Global and Planetary Change 66, 76-84.

Hanebuth, T.J.J, Voris, H.K, Yokoyama, Y., Saito, Y., Okuno, J., 2011. Formation and fate of sedimentary depocentres on Southeast Asia's Sunda Shelf over the past sea-level cycle and biogeographic implications. Earth-Science Reviews 104, 92-110

Heaney, L.R., 1991. A Synopsis of Climatic and Vegetational Change in Southeast Asia. Climatic Change 19, 53–61.

Horozal, S., Chae, S., Seo, J.M., Lee, S.M., Han, H.S., Cukur, D., Kim, D.G., Son, J.H., 2021. Quaternary evolution of the southeastern Korean continental shelf, East Sea: Paleo-incised valley and channel systems. Marine and Petroleum Geology 128, 105011.

Husson, L., Boucher, F.C., Sarr, A.-C., Sepulchre, P., Cahyarini, S.Y., 2019. Evidence of Sundaland's subsidence requires revisiting its biography. Journal of Biogeography 47, 843-853.

Irwanto, D., 2019. Sundaland: Tracing the cradle of civilizations. Indonesia Hydro Media, 386 pp.

Kong, X.H., Liu, J., Du, Y.S., Wen, C., Xu, G., 2011. Seismic geomorphology of buried channel systems in the western South Huanghai Sea: retrodiction for paleoenvironments. Acta Oceanologica Sinica 30, 47-58.

Kurnio, H., Ilahude, D., Prawirasastra, R., Suprijadi, Kuntoro and Arifin, L., 1991. A report of marine geological and geophysical investigation of the Java Sea (Map sheet 1210). Unpublished report.

Lericolais, G., Berne, S., Fenies, H., 2001. Seaward pinching out and internal stratigraphy of the Gironde incised valley on the shelf (Bay of Biscay). Marine Geology 175, 183-197.

Marliyani, G.I., 2016. Neotectonics of Java, Indonesia: Crustal Deformation in the Overriding Plate of an Orthogonal Subduction System. PhD Thesis, Arizona University, 371pp.

Martínez-Carreño, N. and García-Gil, S., 2017. Reinterpretation of the Quaternary sedimentary infill of the Ría de Vigo, NW Iberian Peninsula, as a compound incised valley. Journal of Quaternary Science Reviews 173, 124-144.

Menier, D., Reynaud, J.Y., Proust, J-N., Guillocheau, F., Guennoc, P., Tessier, B., Bonnet, S., Goubert, E., 2006. Basement control on shaping and infilling of valleys incised at the southern coast of Brittany, France. S.E.P.M. Society for Sedimentary Geology, Special Publication 85, 37-55.

Menier, D., Tessier, B., Proust, J.N., Baltzer, A., Sorrel, P., Traini, C., 2010. The Holocene transgression as recorded by incised-valley infilling in a rocky coast context with low sediment supply (southern Brittany, western France). Bulletin de la Société Géologique de France 181 (2), 115–128.

Menier, D., Augris, C., Briend, C., 2014. Les réseaux fluviatiles anciens du plateau continental de Bretagne Sud. Ed. QUAE, 104 p.

Metcalfe, I., 2011. Tectonic framework and Phanerozoic evolution of Sundaland. Gondwana Research, 19(1), pp.3-21.

Mitchum, R.M. and Vail, P.R., 1977. Seismic stratigraphy and global changes of sea-level, part 7. Seismic stratigraphic interpretation procedure. AAPG Memoir 26, 135-143.

Moreira, D.A., Gomes, M.P. & Vital, H., 2019. Shallow sedimentation of Natal shelf and coastal erosion implications, NE Brazil. Geo-Marine Letters 40, 843-851.

Nordfjord, S., Goff, J.A., Austin, J.A., Gulick, S.P.S., 2006. Seismic facies of incised-valley fills, New Jersey continental shelf: implications for erosion and preservation processes acting during latest Pleistocene–Holocene transgression. Journal of Sedimentary Research 76, 1284-1303.

Patmosukismo, S. and Yahya, I., 1974. The basement configuration of the Northwest Java area. Proceeding of the Third Annual Convention, Indonesian Petroleum Association, 129-152.

Posamentier, H.W., 2001. Lowstand Alluvial Bypass Systems: Incised vs. Unincised. AAPG Bulletin 85 (10), 1771–1793.

Posamentier, H.W. and Allen, G.P., 1999. Siliciclastic sequence stratigraphy: concepts and applications. SEPM Concepts in Sedimentology and Paleontology 9, 210 p.

Puchala, R.J., Porębski, S.J., Śliwiński, W.R., August, C.J., 2011. Pleistocene to Holocene transition in the central basin of the Gulf of Thailand, based on geoacoustic survey and radiocarbon ages. Marine Geology 288, 103-111.

Reineck, H.E., Singh, I.B., 1980. Depositional Sedimentary Environments, second ed. Springer-Verlag, New York, 430 pp.

Sarr, A.-C., Husson, L., Sepulchre, P., Pastier, A-M., Pedoja, K., Elliot, M., Arias-Ruiz, C., Solihuddin, T., Aribowo, S., Susilohadi, 2019. Subsiding Sundaland. Geology 47 (2), 119-122.

Sathiamurthy, E., Voris, H.K., 2006. Maps of Holocene Sea Level Transgression and Submerged Lakes on the Sunda Shelf. The Natural History of Chulalongkorn University, Supplement 2:1-43.

Sathiamurthy, E., Rahman, M.M., 2017. Late Quaternary paleo fluvial system research of Sunda Shelf: A review. Bulletin of the Geological Society of Malaysia 64, 81-92.

Shennan, I., 2018. Sea Level Studies – Overview. Reference Module in Earth Systems and Environmental Sciences, Elsevier. https://doi.org/10.1016/B978-0-12-409548-9.11063-2.

Schubel, J.R., 1974. Gas bubbles and the acoustically impenetrable, or turbid, character of some estuarine sediments. In: Kaplan, I.R. (Ed.), Marine Science, Vol. 3. Plenum Press, New York, pp. 275–298.

Smith, D.E., Harrison, S., Firth, C.R., Jordan, J.T., 2011. The early Holocene sea level rise. Quaternary Science Reviews 30, 1846-1860.

Suter, J.R., Berryhill, H.L., Penland, S., 1987. Late Quaternary sea level fluctuations and depositional sequences, Southwest Louisiana continental shelf. In: Nummedal, D., Pilkey, O.H., Howard, S.D. (Eds.), Sea Level Fluctuation and Coastal Evolution. SEPM Special Publication 41, pp. 199 – 219.

Suyanto, F.X. and Sumantri, Y.R., 1977, Preliminary study on the Tertiary depositional patterns of Java: 6th Annual Convention Proceedings Indonesian Petroleum Association 2, 183–213.

Tesson, M., Posamentier, H.W., Gensous, B., 2000. Stratigraphic organization of Late Pleistocene deposits of the western part of the Golfe du Lion Shelf (Langedoc Shelf), western Mediterranean Sea, using high-resolution seismic and core data. American Association of Petroleum Geologists Bulletin 84, 119–150.

Tesson, M., Labaune, C., Gensous, B., Delhaye-Prat, V., 2010. Quaternary compound incised valleys of the Roussillon coast (SE France): correlation of seismic data with core data Bulletin de la Société Géologique de France 181 (2), 183–196.

Tesson, M., Posamentier, H.W., Gensous, B., 2015. Compound incised-valley characterization by high-resolution seismics in a wave-dominated setting: Example of the Aude and Orb rivers, Languedoc inner shelf, Gulf of Lion, France. Marine Geology 367, 1-21.

Thomas, M.A. and Anderson, J.B., 1994. Sea-level controls on the facies architecture of the Trinity/Sabine incised-valley system, Texas continental shelf, in Dalrymple, R.W., Boyd, R., and Zaitlin, B.A., Incised-Valley Systems: Origin and Sedimentary Sequences: SEPM, Special Publication 51, 63–82.

Twarog, M.R., Culver, S.J., Mallinson, D.J., Leorri, E., Donovan, B., Harrison, E.I., Hindes, H., Reed, D., Horsman, E., Shazili, N.A.M., Parham, P.R., 2021. Depositional environments and sequence stratigraphy of post-last glacial maximum incised valley-fill, Malay Basin, northern Sunda Self. Marine Geology 436, 106457.

Voris, H.K., 2000. Maps of Pleistocene sea levels in Southeast Asia: shorelines, river systems and time durations. Journal of Biogeography 27, 1153-1167.

Wang, R., Colombera, L., Nigel, P., Mountey, P., 2020. Quantitative analysis of stratigraphic architecture of incised-valley fills: A global comparison of Quaternary systems. Earth Science Reviews 200, 102988.

Zahirovic, S., Flament, N., Muller, R.., Seton, M., Gurnis, M., 2016. Large fluctuations of shallow seas in low-lying Southeast Asia driven by mantle flow. Geochemistry, Geophysics, Geosystems 17 (9), 3589-3607.

Caption Figures

Figure 1. A: Map showing the spatial distribution and type of vegetation cover in Sundaland during the LGM. Figure adapted from Heaney (1991), Voris (2000) and Bird et al. (2005). **B:** Location of seismic lines in the Java Sea and also shown are the bathymetry contours. **C:** Location of seismic lines and boreholes used in this study from the Jakarta Bay.

Figure 2. A. Map of the Java Sea seafloor sediments. **B.** Map of seafloor sediments of the Jakarta Bay (Harkin, et al., 2004) and geology of the Jakarta-Tangerang area.

Figure 3. Map showing the bathymetry and morphobathymetric features of the Java Sea and the Indian Ocean. Also shown is the drainage basins and the fluvial network of Java. Note the large drainage basins in the north and the smaller basins in the south. The southeastern limit of the Sunda Shelf is visible at the ~110 m

Figure 4. A: Sparker 2D High Resolution Seismic profile L-42. The profile passes through cores BH-02 and BH-07, south to north in the Jakarta Bay. Vertical scale in two-way travel time in seconds (TWTs). The scale in meters is established for sediments with P-wave velocity of 1600 m/sec. **B:** Sparker 2D High Resolution Seismic profile CL-06, west to east in the Jakarta Bay. Vertical scale in two-way travel time in seconds (TWTs). The scale in meters is established for sediments with P-wave velocity of 1600 m/sec.

Figure 5. Sparker 2D High Resolution Seismic profiles C-8, C-7 and C-X. The profile C-8 is located in. Vertical scale is in two-way travel time in seconds (s TWT). The scale is in meters and is established for sediments with P-wave velocity of 1600 m/sec.

Figure 6. Stratigraphic correlation of the facies types recognized in the sediment cores and interpretation of corresponding depositional environments. Also shown are the stratigraphic positions of samples used for AMS ^{14}C dating.

Figure 7. Microfossil assemblages that aided in the interpretation of the depositional environments of the sediments. Benthic foraminifera: 1. *Asterorotalia*; 2. *Operculina*; 3 & 7

Pseudorotalia; 4. *Quinqueloculina*; 5 & 6. *Elphidium*; 8-10. *Ammonia yabei.* Ostracoda: 11. *Phlyctenophora*; 12. *Neocytheretta*; 13. *Loxoconcha*; 14. *Keijella*; 15. *Neomonoceratina*; 16 *Hemicytheridea*

Figure 8. A: Reconstructed paleochannel network of the offshore Java Sea based on High Resolution seismic profiles (location of all lines shown in 1B). **B:** Time slice from the north of the study area at ~72 m subsea showing the principal trunk incised valley and associated components of the fluvial system such as incised dendritic tributary valleys, scroll bars and abandoned meander loops. Figure modified from Posamentier (2001).

Figure 9. Regime diagram showing the global eustatic sea level and Sunda shelf sea level curve for the past 125 ka and 20 ka, respectively, along with timing of the major Marine Isotopic Stages (1–5) and the Last Glacial Maximum. Sunda shelf sea-level curve is adapted from Twarog et al. (2021). Red stars indicate the calibrated ages of sedimentary units (shown with white circles and U7–4) from ^{14}C radiocarbon dating of shells, shell fragments and sediments.

Figure 10. A: Present-day sedimentary architecture of the northern Java Sea. **B:** Schematic depiction of the evolution of incised valley fill in Java Sea, modified from Posamentier (2001). It shows from the time of maximum sea level lowstand, (A) sedimentation was characterized by fluvial deposition, (B) followed by rapid transgression and filling by traction and hemipelagic sedimentation, and finally, (C) the time of sea-level highstand and deposition of hemipelagic drape over the entire area.

List of Tables

Table 1. Locations, water depth and lengths of sediment cores recovered from the the Jakarta Bay and analysed in this study

Table 2. AMS ^{14}C dating of shells, shell fragments and sediments retrieved from the cores

Table 3. Characteristics of acoustic facies and seismic units and their interpretation in terms of depositional environments.

Table 4. Microfossil abundances in BH-02 and BH-07

Figures

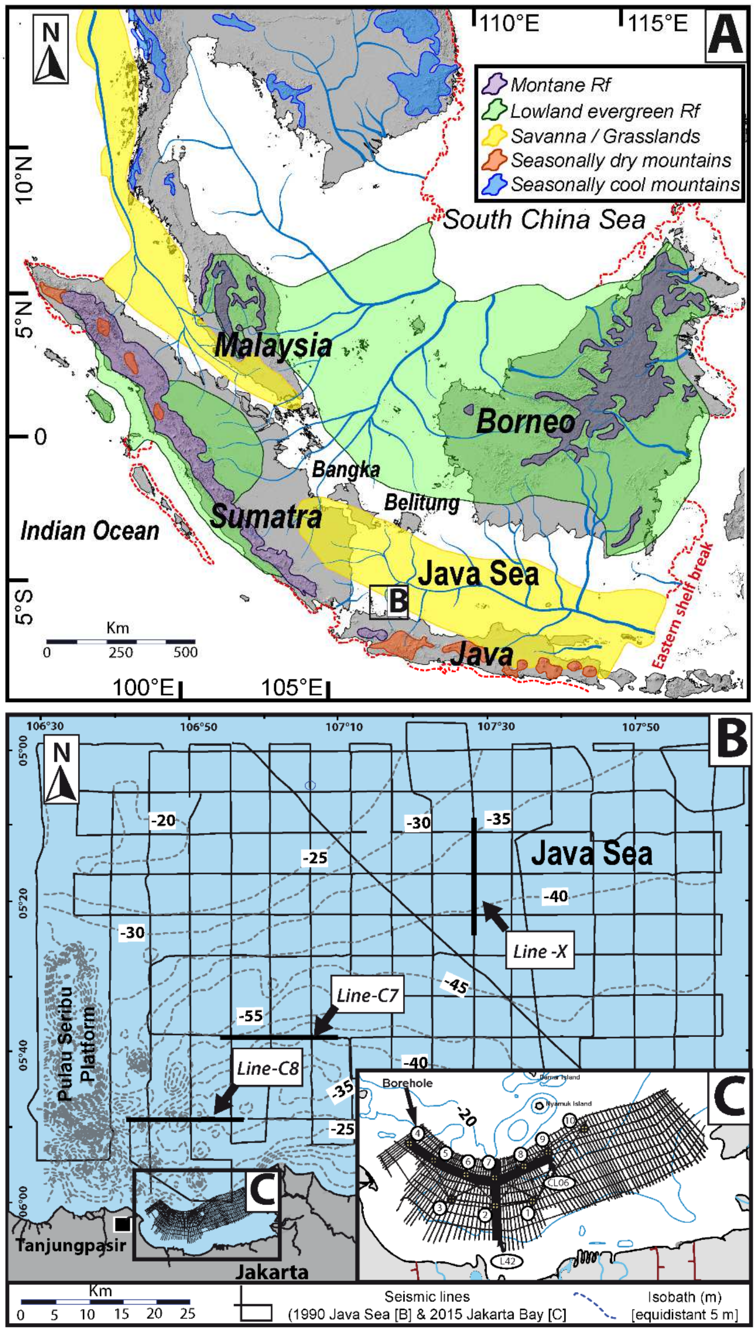

Figure 1. A: Map showing the spatial distribution and type of vegetation cover in Sundaland during the LGM and red dashed line shows the approximate spatial extent of exposed landmass of Sundaland during the LGM. Figure adapted from Heaney (1991), Voris (2000) and Bird et al. (2005). **B:** Location of seismic lines in the Java Sea and also shown are the bathymetry contours. **C:** Location of seismic lines and boreholes used in this study from the Jakarta Bay.

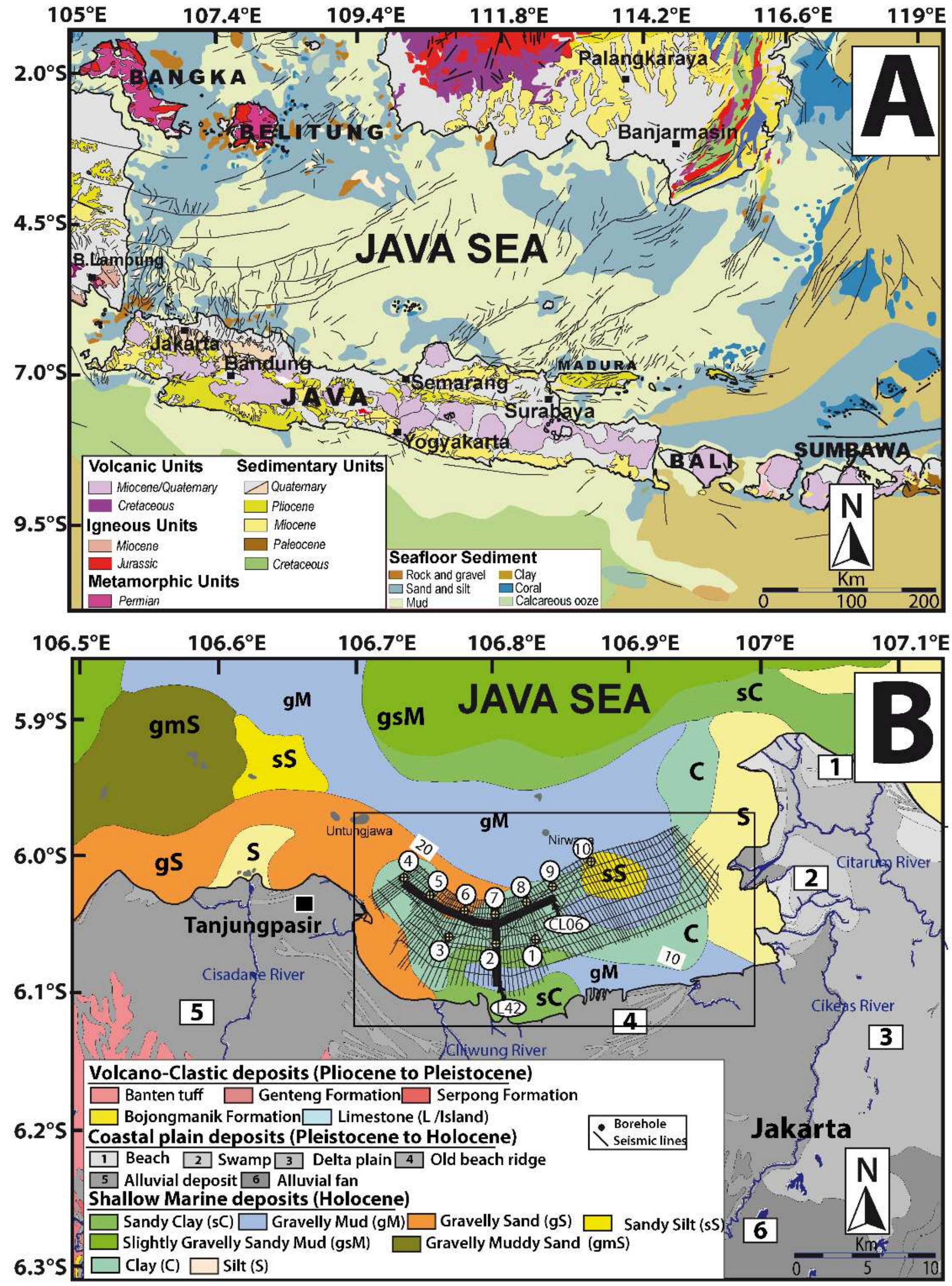

Figure 2. A. Map of the Java Sea seafloor sediments. **B.** Map of seafloor sediments of the Jakarta Bay (Harkin, et al., 2004) and geology of the Jakarta-Tangerang area.

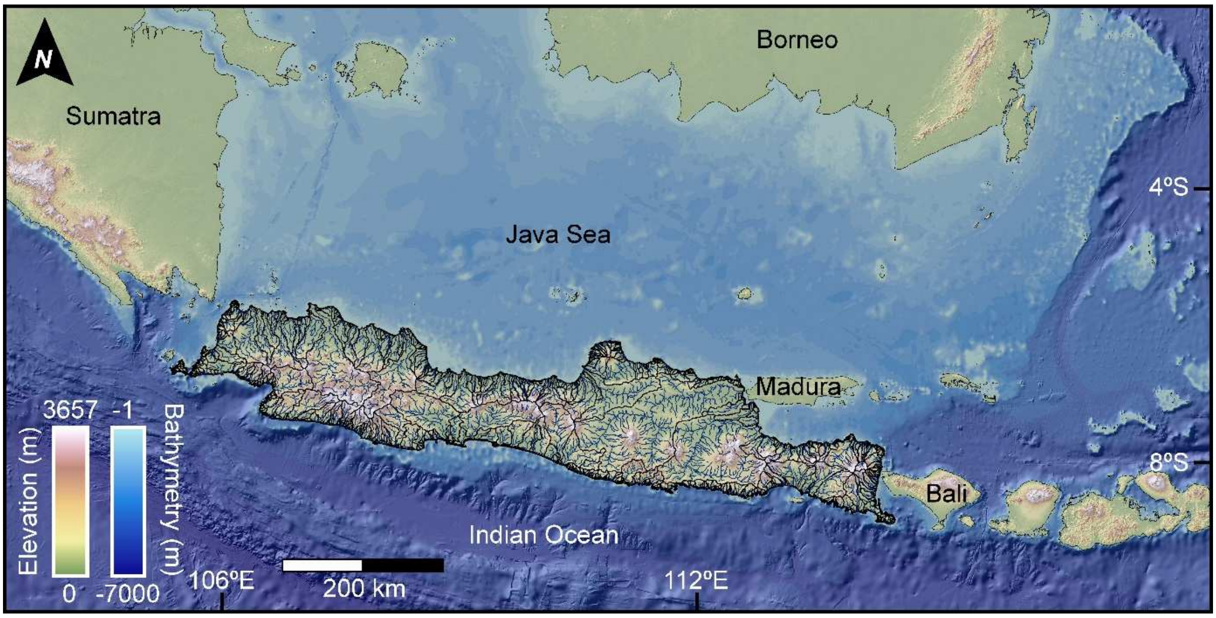

Figure 3. Map showing the bathymetry and morphobathymetric features of the Java Sea and the Indian Ocean. Also shown is the drainage basins and the fluvial network of Java. Note the large drainage basins in the north and the smaller basins in the south. The southeastern limit of the Sunda Shelf is visible at the ~110 m

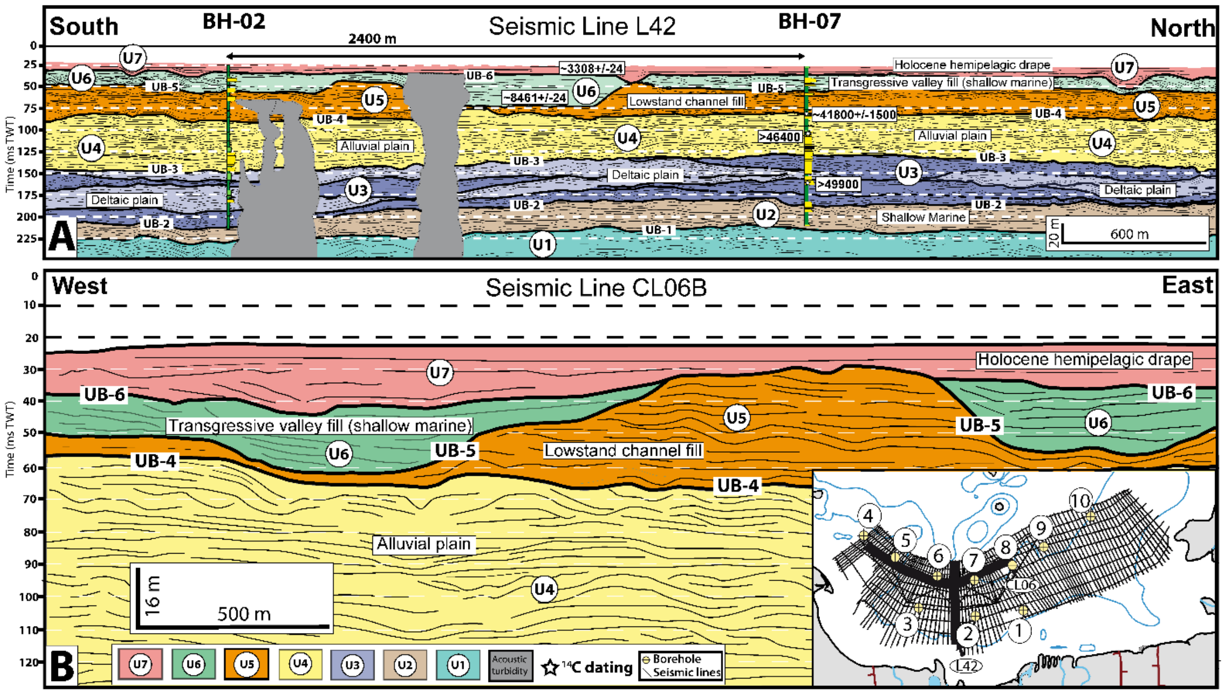

Figure 4. A: Sparker 2D High Resolution Seismic profile L-42. The profile passes through cores BH-02 and BH-07, south to north in the Jakarta Bay. Vertical scale in two-way travel

time in seconds (TWTs). The scale in meters is established for sediments with P-wave velocity of 1600 m/sec. Note that the light blue coloured packages within U3 indicate the head of several deltaic lobes that are stacked and extends laterally. **B:** Sparker 2D High Resolution Seismic profile CL-06, west to east in the Jakarta Bay. Vertical scale in two-way travel time in seconds (TWTs). The scale in meters is established for sediments with P-wave velocity of 1600 m/sec.

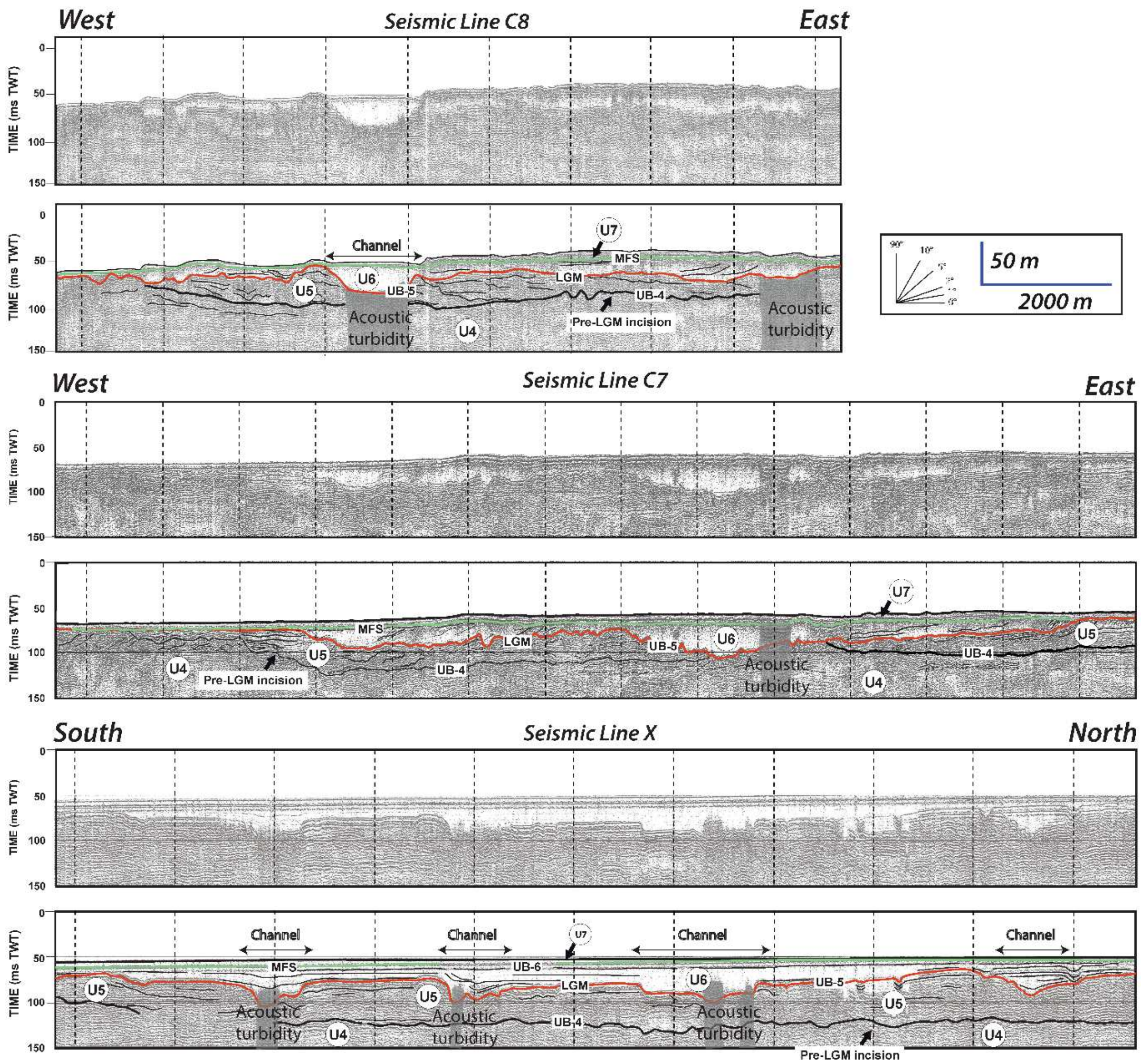

Figure 5. Sparker 2D High Resolution Seismic profiles C-8, C-7 and C-X. The profile C-8 is located in. Vertical scale is in two-way travel time in seconds (s TWT). The scale is in meters and is established for sediments with P-wave velocity of 1600 m/sec.

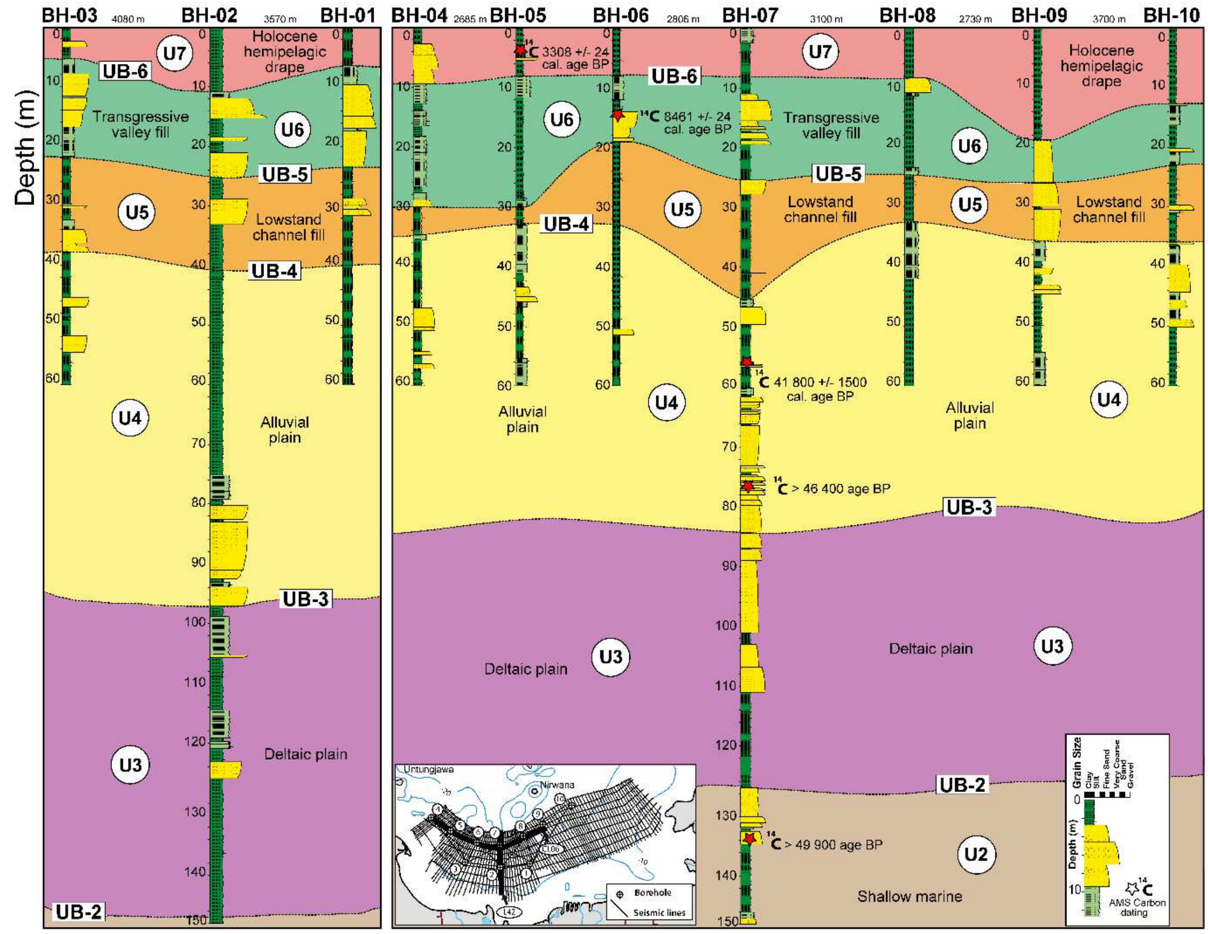

Figure 6. Stratigraphic correlation of the facies types recognized in the sediment cores and interpretation of corresponding depositional environments. Also shown are the stratigraphic positions of samples used for AMS ^{14}C dating.

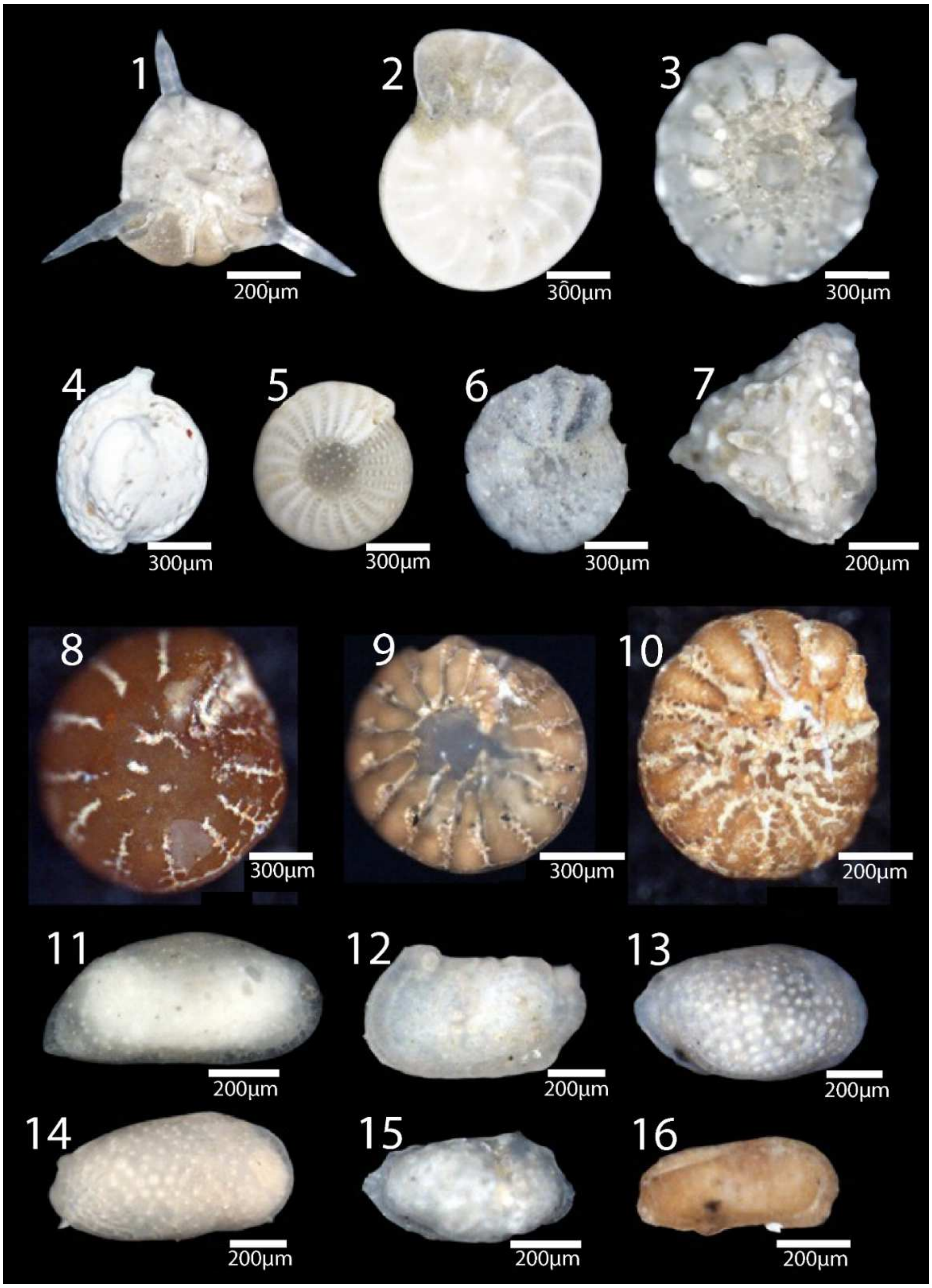
1
200µm
2
300µm
3
300µm
4
300µm
5
300µm
6
300µm
7
200µm
8
300µm
9
300µm
10
200µm
11
200µm
12
200µm
13
200µm
14
200µm
15
200µm
16
200µm

Figure 7. Microfossil assemblages that aided in the interpretation of the depositional environments of the sediments. Benthic foraminifera: 1. *Asterorotalia*; 2. *Operculina*; 3 & 7 *Pseudorotalia*; 4. *Quinqueloculina*; 5 & 6. *Elphidium*; 8-10. *Ammonia yabei.* Ostracoda: 11. *Phlyctenophora*; 12. *Neocytheretta*; 13. *Loxoconcha*; 14. *Keijella*; 15. *Neomonoceratina*; 16 *Hemicytheridea*

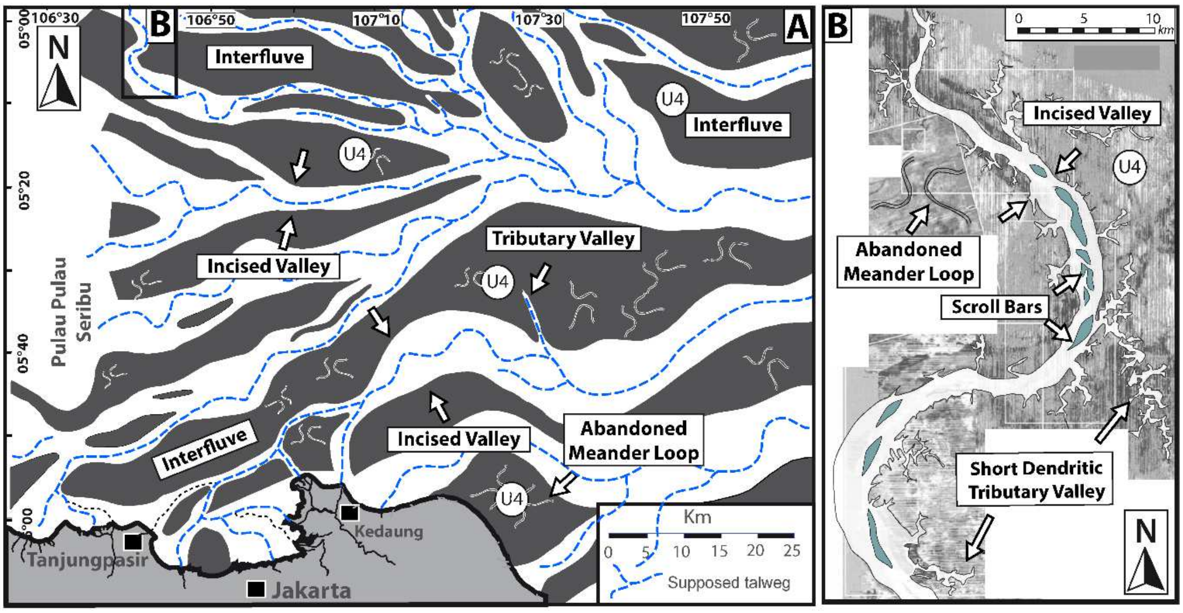

Figure 8. A: Reconstructed paleochannel network of the offshore Java Sea based on High Resolution seismic profiles shown in Figure 1B. **B:** Time slice from the north of the study area at ~72 m subsea showing the principal trunk incised valley and associated components of the fluvial system such as incised dendritic tributary valleys, scroll bars and abandoned meander loops. Figure modified and location from Posamentier (2001)

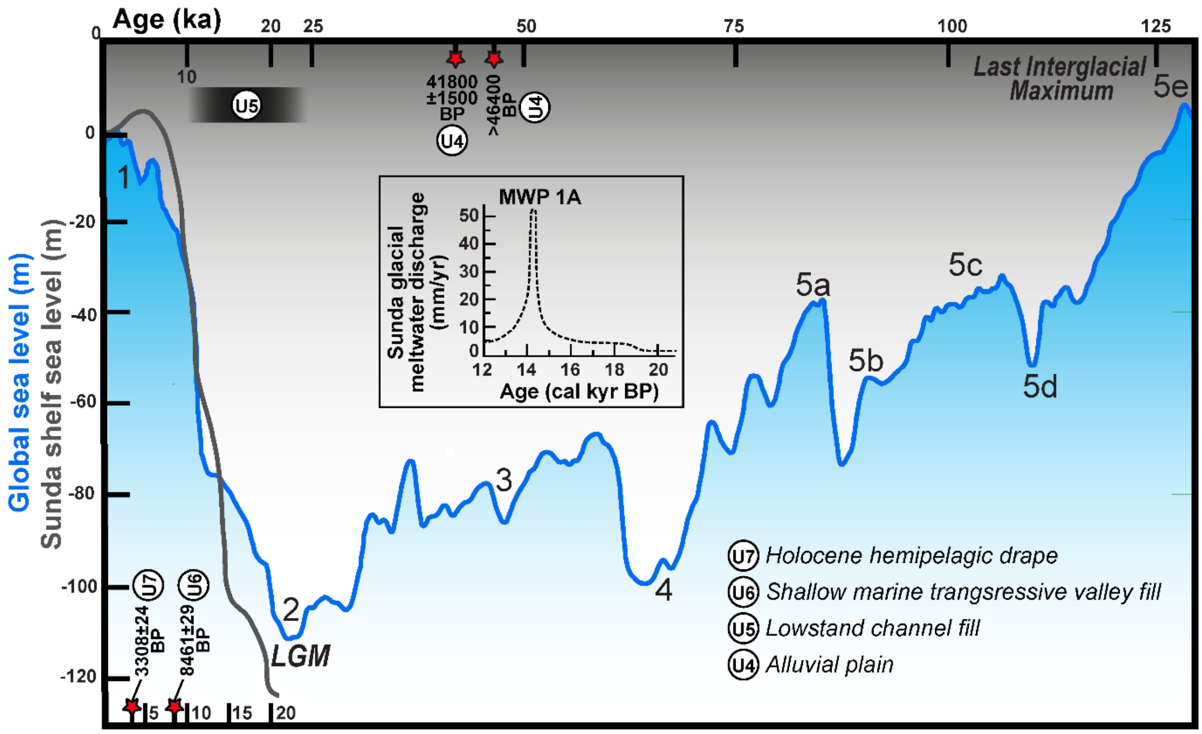

Figure 9. Regime diagram showing the global eustatic sea level and Sunda shelf sea level curve for the past 125 ka and 20 ka, respectively, along with timing of the major Marine Isotopic Stages (1–5) and the Last Glacial Maximum. Sunda shelf sea-level curve is adapted from Twarog et al. (2021). Red stars indicate the calibrated ages of sedimentary units (shown with white circles and U7–4) from ^{14}C radiocarbon dating of shells, shell fragments and sediments.

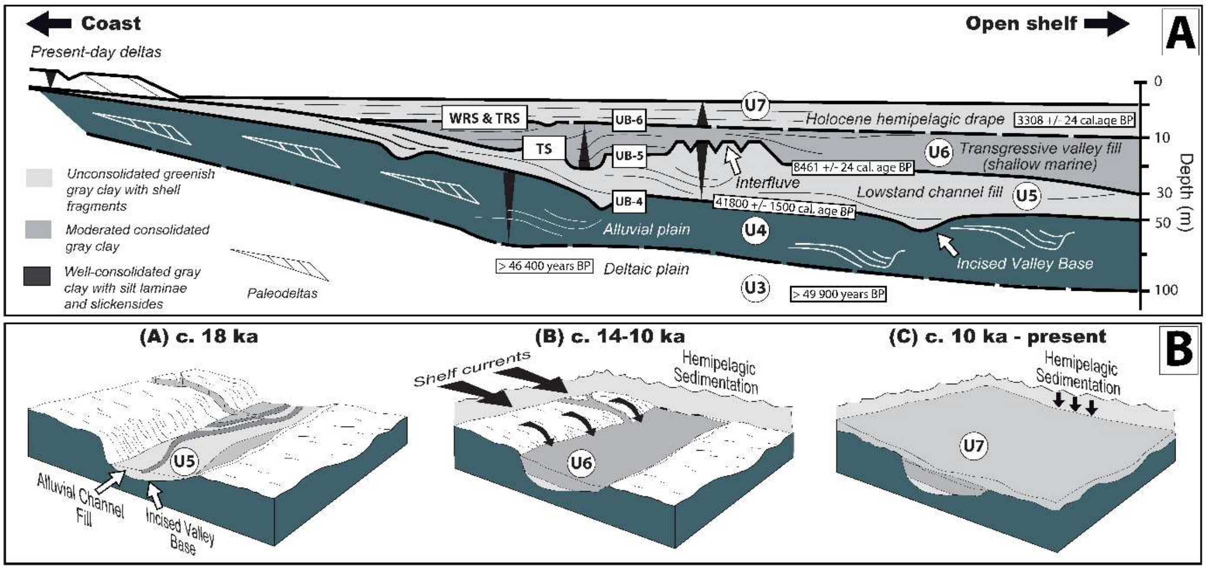

Figure 10. A: Present-day sedimentary architecture of the northern Java Sea. **B:** Schematic depiction of the evolution of incised valley fill in Java Sea, modified from Posamentier (2001). It shows from the time of maximum sea level lowstand, (A) sedimentation was characterized by fluvial deposition, (B) followed by rapid transgression and filling by traction and hemipelagic sedimentation, and finally, (C) the time of sea-level highstand and deposition of hemipelagic drape over the entire area.

Tables

Table 1. Locations, water depth and lengths of sediment cores recovered from the the Jakarta Bay and analysed in this study

Core	Core length (m)	Water depth (m)	Coordinates			
			WGS_1984_UTM_Zone_48S		Latitude (S)	Longitude (N)
			X (m)	Y (m)		
1	60	15.31	704259.24	9330033.60	6°3'28.92"	106°50'43.98"
2	150	14.72	700755.12	9329627.65	6°3'42.52"	106°48'50.09"
3	60	13.76	696699.08	9330108.06	6°3'27.30"	106°46'38.15"
4	60	14.46	692826.95	9335232.98	6°0'40.92"	106°44'31.67"
5	60	15.27	695034.37	9333810.38	6°1'26.97"	106°45'43.62"
6	60	16.54	697886.62	9332414.95	6°2'12.11"	106°47'16.50"
7	150	17.36	700646.47	9332020.42	6°2'24.64"	106°48'46.28"
8	60	18.23	703556.3	9334974.58	6°1'49.40"	106°50'20.78"
9	60	19.59	705541.07	9334974.41	6°0'47.30"	106°51'25.11"
10	60	20.49	708651.68	9336919.69	5°59'44.30"	106°53'6.01"

Table 2. AMS ^{14}C dating of shells, shell fragments and sediments retrieved from the cores

Core	Lab number	Depth (mbss)	Seismic Unit	d13C value	Age (^{14}C years BP)	Material
BH-05	X32132	7	U7	3.5	3308±24	Shell
BH-06	X32133	14.3	U6	-4.0	8461±29	Shell
	X31404	56.2	U4	-29.1	41800±1500	Sediment and shell fragments
BH-07	X31405	77.00	U4	-19.2	>46400	Sediment and shell fragments
	X31406	134.45	U2	0.8	>49900	Sediment and shell fragments

Table 3. Characteristics of acoustic facies and seismic units and their interpretation in terms of depositional environments.

Unit	Facies	Illustration	Continuity	Amplitude	Frequency	Reflector Configuration	Interpretation
U-7	F-7A		Good	Good	Medium	Aggrading parallel	Marine muds
	F-7B		Medium	Good	Medium	Aggrading parallel	Channel fill
U-6	F-6A	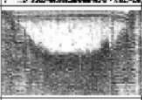	Poor	Very poor	Low	Transparent	Channel infill polymix
	F-6B	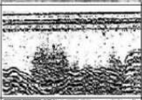	Poor	High	Low	Acoustic turbidity	Gas-charged sediments
	F-6C	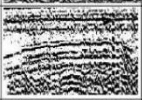	Poor	Medium	High	Aggrading parallel	Bars associated to channel migration
U-5	F-5A		Very poor	Medium	Low	Acoustic turbidity	Gas-charged sediments
	F-5B		Poor	Medium	High	Oblique-aggrading subparallel	Channel bars system
	F-5C	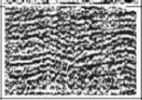	Poor	High	High	Oblique-aggrading subparallel	Channel bars system
U-4	F-4A	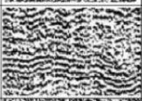	Medium	Medium	High	Aggrading subparallel	Bars associated to channeling drainage system
	F-4B	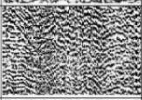	Poor	Medium	Medium	Acoustic turbidity	Gas-charged sediments
	F-4C	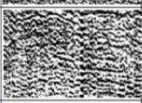	Poor	Poor	Medium	Irregular Oblique-aggrading subparallel	Bars associated to channeling drainage system
U-3	F-3A		Medium	Medium	Medium	Aggrading sub parallel	Marine muds and sandy intercalation
	F-3B	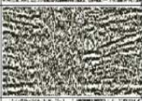	Very poor	Medium	Medium	Acoustic turbidity	Gas-charged sediments
U-2	F-2A		Medium	Medium	Low	Aggrading folded parallel	Marine muds
	F-2B		Very poor	Medium	Low	Acoustic turbidity	Gas-charged sediments
U-1	F-1A		Low	Medium	Low	Aggrading sub-parallel	Marine sediments
	F-1B	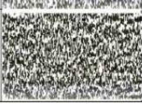	Very poor	Low	Low	Acoustic turbidity	Gas-charged sediments

Table 4. Microfossil abundances in BH-02 and BH-07

BH-02 — Ostracod

BH-02 depth below seafloor (m)	*Actinocythereis*	*Argilloecia*	*Atjehella semiplicata*	*Bairdopillata*	*Caudites*	*Cytherella*	*Cytherelloidea*	*Hemicytheridea*	*Keijella*	*Keijia*	*Lanckacythere*	*Mycyprideis*	*Neomonocertina*	*Loxoconcha*	*Phlyctenophora*	*Pistocythereis*	*Psammocythere*	*Stigmatocythere*	Other
3,20			○			○	○	Ѧ	●		∘		●	©	Ѧ	∘		©	
7,18	∘	∘	∘		○	○		●	●				©	Ѧ	●	○			∘
11,03								○	∘					∘					
20,90	○					∘	∘	○	Ѧ			Ѧ	○	∘		Ѧ			
27,25																			
41,00																			
42,00																			
54,65																			
71,00									○										
110,70	○							©	©				○						
120,00	∘																		
128,50	∘	©	○	○		Ѧ	©	Ѧ	©	©			©	○			∘	○	∘
134,64		○	○	∘	∘	○	∘	○	○	○			∘	○					

BH-02 — Benthic foraminifera

BH-02 depth below seafloor (m)	*Ammonia*	*Amphistegina*	*Asterorotalia*	*Brizalina*	*Cancris*	*Dendritina*	*Discopulvinulina*	*Elphidium*	*Florilus*	*Lagena*	*Operculina*	*Pseudorotalia*	*Quinqueloculina*	*Rotalia*	*Shlumbergerella*	*Spiroloculina*	*Triloculina*	Other	*Remarks*
3,20	●						○	●	Ѧ	∘		©	Ѧ	○	∘	∘			Shallow marine environment
7,18	●		○			©		●			●		●			©	∘	∘	
11,03								©					○						
20,90	○		●					Ѧ		∘	○	©	©			∘		○	
27,25																			land
41,00																			
42,00																			
54,65								∘				●	∘						Shallow marine environment
71,00			○									∘							
110,70	●		∘									○	∘						
120,00			∘					∘				∘	∘					∘	
128,50	Ѧ		●	○	∘		○	○		○	●	©	Ѧ			○		∘	
134,64	Ѧ	∘	Ѧ					©			●	○	©			∘			

Notes:
Biogenic
Rare (R) : 1 ∘
Few (F) : '2-5 ○
Common (C) : 6-10 ©
Abundant (A) : 11-25 Ѧ
Very abundant (VA) >25 ●


3.20 m


27.25 m

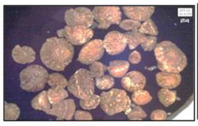
54.65m


110.70m


134.64 m

BH-07 — Ostracod

BH-07 Depth below seafloor (m)	*Actinocythereis*	*Argilloecia*	*Atjehella*	*Cytherella*	*Cytherelloidea*	*Cyheropteron*	*Hemicytheridea*	*Keijella*	*Keijia*	*Neomonocertina*	*Neocytheretha*	*Loxoconcha*	*Phlyctenophora*	*Pistocythereis*	*Stigmatocythere*	*Mycyprideis*	*Other*
2,10	©	○	∘	○	©	∘	Ѧ	○	○	○	∘	∘	Ѧ	∘	○		∘
3.18	○			∘			○	∘			∘		∘	∘			
22.68	∘	○	○	∘	○		©	●		Ѧ	○	○	Ѧ	●	∘	○	∘
23.40	○	∘	○	∘			©	●		●	○	©	Ѧ	Ѧ	∘	○	∘
23,85	©	©	©		○		Ѧ	●	∘	©	∘	∘	69	©	○	©	∘
26,10													○				
27,45																	
27,50																	
28,30																	
31,80	○			∘						∘			○	∘	∘		
32,62																	
33,45																	
38,30																	
40,75																	
53,27																	
55,65	○						○	∘					○	∘			
56,20																	
65,11																	
68,55																	
71,72																	
77,00																	
98,40	○			○			○	○							○		∘
101,10	○			©	○		○	Ѧ					∘	©	○		
132,84					○				○		○						
134,45																	
136,55				Ѧ	○		○	©	○		○						
141,10																	
149,41			∘	○	©			©	∘		∘						

BH-07 — Benthic foraminifera

BH-07 Depth below seafloor (m)	*Ammonia*	*Asterorotalia*	*Brizalina*	*Cancris*	*Cibicides*	*Dendritina*	*Elphidium*	*Florilus*	*Lenticulina*	*Operculina*	*Pseudorotalia*	*Quinqueloculina*	*Spiroloculina*	*Triloculina*	*Other*	*Remarks*
2,10		○				Ѧ	●			Ѧ	∘	●	Ѧ	∘	○	shallow marine-reef environments
3.18		○				Ѧ	●			Ѧ	Ѧ	Ѧ				
22.68		●					●			∘	○	∘	○		∘	
23.40																
23,85	○	∘					●			∘		Ѧ	○	∘		
26,10	∘					○	○			©		∘				nearshore
27,45						○	○			○						
27,50																
28,30										∘						
31,80		○			∘		Ѧ			○	○	Ѧ	○			
32,62						∘	○			∘		○				
33,45																
38,30										∘						nearshore
40,75							○			○	∘	∘				
53,27						Ѧ	Ѧ			©	©	○				
55,65		∘					●			©	©	©	○		Ѧ	
56,20																Barren zone, no ostracod n foram, quartz sand, organic materials
65,11																
68,55																
71,72																
77,00																
98,40	●	©	∘	∘			Ѧ					©			∘	Shallow marine-reef environments
101,10	Ѧ	●					©	∘	∘		○	©	○	○		
132,84	Ѧ	○					34			○	○	©			Ѧ	
134,45	●	●									>>					
136,55	●	●	∘	∘			○					∘				
141,10	∘	○		∘			∘		○		©	∘			○	
149,41	©	●					○				©	∘				

Biogenik
Rare (R) : 1 ∘
Few (F) : '2-5 ○
Common (C) : 6-10 ©
Abundant (A) : 11-25 Ѧ
Very abundant (VA) >25 ●


2.10 m


23.40 m


33.40 m


77.00 m


98.40 m

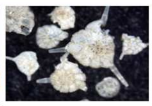
149.41 m